Modeling the indentation size effects of polymers, based on couple stress elasticity and shear transformation plasticity

Chao Peng[a], Fanlin Zeng[a*]

[a] Department of Astronautic Science and Mechanics, Harbin Institute of Technology, Harbin 150001, People's Republic of China

Abstract

This work attempts to find out the models which can describe the size effects in modulus and hardness of polymers measured by indentation tests. Firstly, the elastic size effects are described by a model, through introducing a model of elastic unloading load with consideration of couple stress elasticity into the Oliver-Pharr indentation approach. The accordingly proposed modulus model and hardness model agree excellently with a large amount of experimental data obtained from literatures. The models show that the elastic size effects of polymers and their experimental observations are mainly determined by the molecular structures. The fitting results verify that the size effects in indentation hardness of polymers with complex molecular structures are significantly elastic. Secondly, it is postulated that the plastic size effects in indentation hardness of polymers are only derived from their glassy components. A shear transformation plasticity theory proposed for glassy polymers is employed to characterize the plastic size effects. A hardness model is accordingly proposed and agrees well with related experimental data.

1. Introduction

The nano-indentation approach of Oliver and Pharr [1] has been widely used to measure modulus and hardness of crystals, polymeric materials or thin films. In such a test, the phenomenon that the measured modulus and hardness increase with decreasing indentation depths is called indentation size effects (simplified as ISEs). For crystals, size effects almost do not emerge in indentation modulus, but mainly in indentation hardness, and have been well studied and mostly described by the model proposed by Nix and Gao [2]. Nix and Gao found ISEs of crystals are induced by the different distribution of geometrically necessary dislocations along the indentation depths. For polymers, size effects are however extensively observed in both indentation modulus and indentation hardness [3-10]. But the notion of dislocations cannot be applied to polymers due to the lack of long-range order. It is necessary to investigate the essential mechanism of the size effects of polymers, from which we may get some favorable results conducive to the development of MEMS, sensors, precision instruments.

The present work attempts to construct models which can describe the ISEs of polymers. The first study in this respect is the hardness model of Lam and Chong [11] which adopts the notion of the geometrically necessary kinks of molecular chains in polymer plasticity. This is similar to the innovation of Nix and Gao[2] which adopts the notion of the geometrically necessary dislocations in crystal plasticity. Recently, Han and Nikolov [12] and Alisafaei et al. [13] pointed out that the size effects in indentation modulus (simplified as modulus ISEs) of polymers are only elastic size effects, because the determinations of modulus in indentation tests are only related to elastic deformations. They also suggested the size effects in indentation hardness (simplified as hardness ISEs) of polymers can be decomposed into elastic part and plastic part, and the elastic part probably even be dominant due to the extensive elasticity of polymers. In order to theoretically characterize the ISEs of polymers, Han and Nikolov [12] simplified the indentation problem as the Boussinesq problem. The couple stress elasticity is introduced into the simplified problem and a hardness model is accordingly proposed. Both the model of Lam and Chong [11] and that of Han and Nikolov [12] involve rotation gradients in deformations of microstructures. Voyiadjis et al. [10] suggested that the size effects of polymers may be at least partly independent of rotation gradients, since size effects were also found in rotation-free situations such as uniaxial tensile experiments of polymeric nanofibers. They accordingly proposed a hardness model, by employing a shear transformation

plasticity theory of glassy polymers which was developed by Voyiadjis and Samadi-Dooki [14].

The present work is an extension of the works of Han and Nikolov [12] and Voyiadjis et al. [10]. Before we attempted to solve the spherical contact problem in the context of couple stress elasticity a number of solutions regarding the same problem have been reported [15-18]. Based on these works, similar to the work of Han and Nikolov[12], the couple stress elasticity was introduced into Hertz contact problem, and a theoretical model of contact load which can characterize the size effects in contact tests of elastomers was derived [19] in our previous work. In Section 2, the Oliver-Pharr indentation approach is firstly recalled. Then the proposed load model is introduced into Oliver-Pharr approach. Accordingly, two models respectively characterizing the modulus ISEs and the elastic hardness ISEs are derived. These two models are applied to a large number of experimental data to illustrate their validity. In Section 3, the shear transformation plasticity theory and hardness model respectively proposed by Voyiadjis and Samadi-Dooki[14] and Voyiadjis et al.[10] are recalled. A new hardness model with less assumptions and in a simpler form is proposed, in order to characterize the plastic hardness ISEs of polymers. The proposed hardness mode is compared with related experimental data.

2. Model for the elastic indentation size effects of polymers

2.1. Model development

We start by recalling the indentation approach proposed by Oliver and Pharr [1]. Their approach adopts a diamond Berkovich indenter. A single indentation cycle contains three periods: loading to a peak load P_{max}, as shown in Fig. 1(a); holding for a period of time at the peak load; unloading from the peak load to zero with a plastically residual depth h_f being left, as shown in Fig. 1(b). The holding period is conducted in order to minimize any non-elastic effects upon unloading period, assuring a completely elastic deformation with respect to $h-h_f$. Fig. 1(c) shows a typical load-curve of a single indentation cycle. Three important quantities are recorded: the maximum deformation depth h_{max}, the peak load P_{max} and the plastically residual depth h_f.

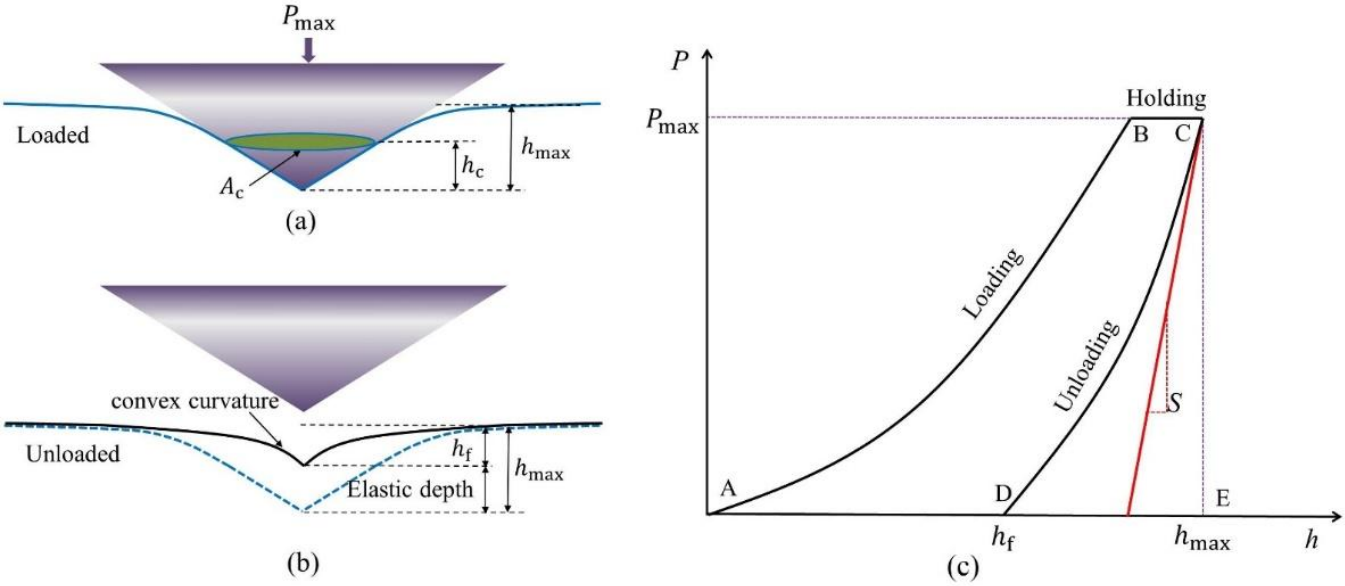

Fig. 1. (a) The Berkovich indenter is pressed into the sample and holding it for a period of time; (b) Unloading the indenter at the contact depth h_c and the maximum deformation depth h_{max}; After unloading, a residual depth h_f and an impression with convex curvature are left on the surface; (c) The loading and unloading curves of a single indentation cycle, in which the red line schematically illustrates the contact stiffness that is defined as the slope of the initial portions of the unloading curve.

Oliver-Pharr approach starts with the elastic contact analysis at the initial unloading stages. They found that the elastic unloading curve can be best fitted by a power law relation:

$$P = \alpha (h - h_f)^m, \tag{1}$$

where P is the elastic contact load at the unloading stage, α and m are fitted parameters and h_f is exactly the plastic residue. The critical property estimated from the unloading curve is the elastic contact stiffness at initial unloading stages, which is defined as

$$S = \left.\frac{dP}{dh}\right|_{h_{max}}. \tag{2}$$

The contact depth h_c shown in Fig. 1(a) is then estimated by

$$h_c = h_{max} - 0.75\frac{P_{max}}{S}. \tag{3}$$

The projected area of elastic contact shown in Fig. 1(a) is determined by substituting h_c into the area function of the cross section of indenter, i.e.,

$$A_c = 24.5h_c^2 \tag{4}$$

and the elastic modulus is related to A_c by

$$E = \frac{\sqrt{\pi}(1-\nu^2)}{2}\frac{1}{\beta_0}\frac{S}{\sqrt{A_c}}, \tag{5}$$

where β_0 is a dimensionless parameter accounting for indenter geometry. Finally, the hardness is determined by

$$H = \frac{P_{max}}{A_c}. \tag{6}$$

The critical advance in Oliver-Pharr approach is their understanding of the effective behavior of Berkovich indenter at the initial unloading stages. Firstly, on the basis of a large number of experimental observations, they found the elastic unloading curves at the initial stages can be exactly represented by Eq. (1), in which the values of m are around 1.5. The contact load of linear elastic half space by a rigid paraboloid of revolution has been analytically expressed by Sneddon [20] as a power law with the exponent being exact 1.5. Therefore, Oliver and Pharr suggested the effective behavior of the Berkovich indenter in contact with the elastic recovery of deformed surface can be approximated by the behavior of a paraboloid of revolution in contact with the flat surface of half space, as schematically shown in Fig. 2. Further, on the basis of several finite element simulations, Pharr and Bolshakov [21] verified this inference and constructed the concept of "effective indenter shape".

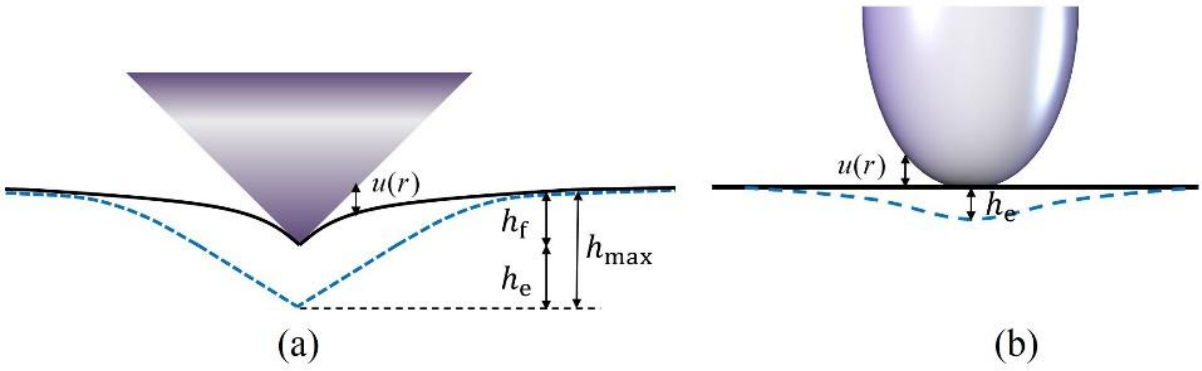

Fig. 2. (a) A Berkovich indenter in contact with the elastic recovery of a plastic impression; (b) A paraboloid of revolution in contact with the flat surface of elastic half space.

In Sneddon's work, the contact load of linear elastic half space by a rigid paraboloid of revolution is expressed as

$$P_0 = \frac{8\mu\sqrt{R}}{3(1-\nu)}h_e^{\frac{3}{2}} \tag{7}$$

where P_0 is the linear elastic contact load, μ is the shear modulus of half space, R is the curvature radius of indenter tip, ν is Poisson ratio, h_e is the normal displacement of the contact center. In the limit of small displacement, this contact problem is the same as the contact of half space by a rigid sphere, which is also the famous Hertz contact problem [22].

Recently, we investigated the Hertz contact problem in the context of couple stress elasticity [19]. A model of contact load with consideration of couple stress effects is analytically derived and expressed as

$$P = P_0\left[1+\frac{3(1-\nu)l^2}{2Rh_e}\right]. \tag{8}$$

where P is the couple stress-based contact load, l is a characteristic length of deformation body employed in couple stress elasticity to characterize size-dependent deformations, similar to the two Lamé constants in classical linear elasticity. It can be seen from Eq. (8) that the couple stress-based contact load P contains an augmenting term relative to the linear elastic contact load P_0. Besides, the augmenting effects increase with the decreasing deformation depth h_e, which denotes the size effects existing in contact load. Furthermore, this equation has been successfully used to characterize the size effects found in spherical contact test of PDMS [23].

The above discussion indicates the modulus ISEs and the elastic part of hardness ISEs may be theoretically modeled by introducing the couple stress-based elastic contact formula Eq. (8) into the Oliver-Pharr indentation approach. Specifically, the elastic contact load at the initial unloading stages, i.e., Eq. (1), may be decomposed into two parts: a linear elastic load and a corresponding augment mediated by couple stress effects, similar to Eq. (8). For simplicity, the linear elastic part in Eq. (1) is assumed to be in the same analytical form as Eq. (7), with the exponent m in Eq. (1) being sustained. Besides, the couple stress-mediated load augment is assumed to be the same as that in Eq. (8), i.e., $4\mu l^2(h-h_f)^{1/2}/\sqrt{R}$. Based on these considerations, the couple stress-based unloading curve can be expressed as

$$P = \frac{8\mu\sqrt{R}}{3(1-\nu)}(h-h_f)^m\left[1+\frac{3(1-\nu)l^2}{2R(h-h_f)^{m-\frac{1}{2}}}\right]. \tag{9}$$

Incorporating Eq. (9) into Eq. (2), the couple stress-based contact stiffness can be expressed as

$$S = S_0\left[1+\frac{3(1-\nu)l^2}{4mR(h_{max}-h_f)^{m-\frac{1}{2}}}\right], \tag{10}$$

where S_0 is the linear elastic contact stiffness, which is obtained by incorporating the leading term in Eq. (9) into Eq. (2), and expressed as

$$S_0 = \frac{8m\mu\sqrt{R}(h_{max}-h_f)^{m-1}}{3(1-\nu)}. \tag{11}$$

According to Eq. (5), the size effects in modulus can only come from S and A_c, because other parameters in Eq. (5) are prescribed constants. Eq. (10) has introduced the size effects versus $h_{max}-h_f$ into S. Similarly, the size effects could be introduced into A_c by incorporating Eq. (9) and Eq. (10) into Eq. (3). However, the respective size effects in P and S may be largely "faded" after they are incorporated into the term P/S, due to the quotient form of this term. Additionally, this incorporation would make the expression of the resultant model of A_c much complex. Based on these considerations, for simplicity the size effects in A_c are neglected here. Therefore, the size effects in modulus are modeled by directly incorporating Eq. (10) into Eq. (5), and expressed as

$$E = E_0\left[1+\frac{3(1-\nu)l^2}{4mR(h_{max}-h_f)^{\zeta-\frac{1}{2}}}\right], \tag{12}$$

where E_0 is the linear elastic indentation modulus, which is obtained by incorporating Eq. (11) into Eq. (5).

Eq. (12) describes the modulus ISEs as that the modulus varies with the completely elastic depth $h_{max}-h_f$. However, in an indentation test, the measured modulus and hardness are recorded as a function of h_{max}. Therefore, in order to apply Eq. (12) to the experimentally obtained moduli, it should be also expressed as a function of h_{max}. In the indentation tests of UHMWPE, PS and PMMA [3] and PAI [7], the fraction of elastic deformation work (the area encompassed by CDE in Fig. 1(c)) in total deformation work (the area encompassed by ABCE in Fig. 1(c)) is found to approximately remain constant as h_{max} increases, as can be seen in Fig. 3. Therefore, for simplicity we assume that the elastic recovery $h_{max}-h_f$ is related to h_{max} by a relation: $(h_{max}-h_f)/h_{max}=\eta_e$, where the constant η_e essentially denotes the fraction of elastic depth, ranging from 0 to 1. Based on these approximations, we can express Eq. (12) in the form of

$$E = E_0\left[1+\frac{l_R}{2mh_{max}^{m-\frac{1}{2}}}\right], \tag{13}$$

where the relevant parameters are combined into a higher-order parameter l_R by

$$l_R = \frac{3(1-\nu)l^2}{2R\eta_e^{m-\frac{1}{2}}}. \tag{14}$$

As the constant fraction η_e is dimensionless, the higher-order parameter l_R has a dimension of length. So far, the modulus ISEs have been characterized by the exponent m and the higher-order parameter l_R. According to the understanding of effective behavior of indenter in the work of Oliver and Pharr [1], the theoretical range of m is considered to be around 1.5, at most ranging from 1 to 2. In a difference to m, to determine the theoretical range of l_R is of difficulties, because l_R contains five pieces of information, either from the material itself or from the indenter.

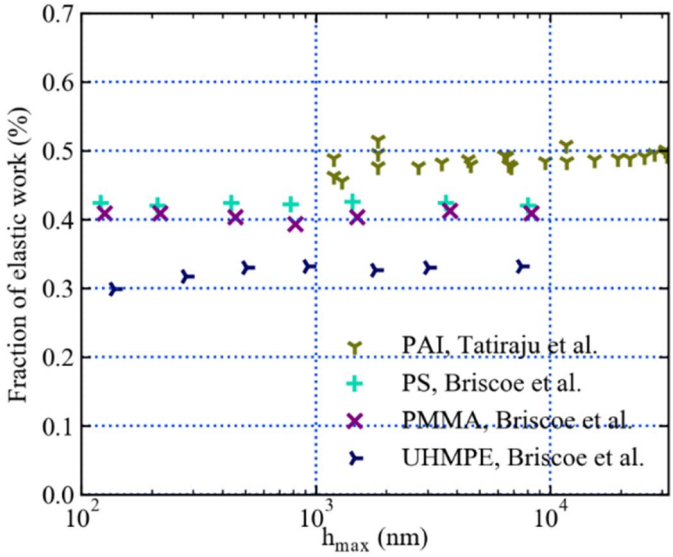

Fig. 3. The fraction of elastic deformation work in total deformation work of UHMWPE, PS and PMMA [3] and PAI [7].

As mentioned in Section 1, Han and Nikolov [12] and Alisafaei et al. [13] pointed out the hardness ISEs of polymers can be decomposed into elastic part and plastic part, and the elastic part may even be dominant. If the plastic hardness ISEs are temporarily neglected here, the elastic part can be similarly modeled by incorporating the couple stress-based elastic contact load, i.e., Eq. (9), into the hardness formula Eq. (6). Therefore, we can obtain

$$H = H_0\left[1+\frac{l_R}{h_{max}^{m-\frac{1}{2}}}\right], \tag{15}$$

where H_0 represents the macro hardness or constant hardness, which is obtained by substituting linear elastic contact

load (the leading term in Eq. (9)) into Eq. (6) with h being $h_{\max}$. The parameters l_R and m are exactly those in Eq. (13). However, it should be noted that if this hardness model is directly applied to the experimental data of indentation hardness of a polymer, the estimated values of l_R and m may respectively deviate from those estimated by Eq. (13), because the plastic hardness ISEs in experimental data may be non-negligible and even significant. The same values as those estimated by Eq. (13) can be obtained only if the plastic hardness ISEs of this polymer can be extremely negligible.

So far, the modulus ISEs and the elastic hardness ISEs are respectively modeled by Eq. (13) and Eq. (15). It can be found from Eq. (13) and Eq. (15) that a relation exists between the two augmenting effect terms in the two models, which can be expressed as

$$\frac{H-H_0}{H_0}=2m\left(\frac{E-E_0}{E_0}\right). \tag{16}$$

As mentioned above, if the plastic hardness ISEs of a polymer can be extremely negligible, the values of l_R and m estimated by Eq. (13) will be the same as those estimated by Eq. (15). Under this condition, if the experimentally obtained hardness and moduli are respectively processed in the form of Eq. (16) and plotted in a form versus $1/h_{\max}$, two power law curves with uniform exponent $m-0.5$ will be obtained. In particular, these two curves become two straight lines if the values of m are uniformly estimated as 1.5, which requires the "effective indenter shape" in tests is equivalent to ad paraboloid of revolution. Additionally, there is a proportional relationship of 3 times between the slopes of the two lines.

2.2. Model verification

The scattering points in Fig. 4 are experimentally obtained indentation moduli of various glassy polymers including PS (Briscoe et al. [3]), PMMA (Briscoe et al. [3]; Voyiadjis et al. [10]), Epoxy (Alisafaei et al. [8]), and various semi-crystalline polymers including Nylon66 (Shen et al. [6]), UHMWPE (Briscoe et al. [3]), PTFE (Li and Bhushan [24]) and LDPE (Tavares et al. [5]). Fig. 5(a-d) correspondingly shows the indentation hardness of these polymers. In addition, Fig 5(e-f) shows the indentation hardness of Epoxy (Chong and Lam[4]), PC (Chong and Lam [4]; Samadi-Dooki et al. [9]) and PAI (Tatiraju et al. [7]). The moduli of polymers shown in Fig. 5(e-f) were not measured in the respective literatures. It can be seen from these two figures that for PS, PMMA, Epoxy (Alisafaei et al. [8]), Nylon66 and LDPE the hardness ISEs are always accompanied by the modulus ISEs, while for UHMWPE and PTFE the ISEs arise in neither modulus nor hardness. In other words, for these polymers, ISEs must arise in hardness as long as it arises in modulus, or vice versa.

In order to illustrate the validity of Eq. (13) and Eq. (15) for characterizing ISEs of polymers, they are respectively fitted to the experimental data with size effects shown in Fig. 4 and Fig. 5. As shown in the two figures, an excellent agreement between the two models and the experimental data of polymers other than Epoxy (Alisafaei et al. [8]) is obtained. For Epoxy (Alisafaei et al. [8]), both Eq. (13) and Eq. (15) slightly deviate from the experimental data after depths of about 1000 nm, i.e., larger E_0 and H_0 are predicted. This may be attributed to the continuous declines of experimental data at these depths, due to the possible inhomogeneity of properties derived from sample preparation.

The fitted values of E_0, l_R and m in Fig. 4 and Fig. 5 are shown in Table 1 and Table 2, respectively. It can be seen that all m values in Table 1 are in the theoretical range of m. Specially, the m values of PS and PMMA (Briscoe et al. [3]) are significantly close to 1.5, which implies that the "effective indenter shape" used in these experiments can be well identified as a paraboloid of revolution. Additionally, in Table 1 the l_R value of LDPE is larger than those of other polymers. Comparing Table 2 with Table 1, it can be found that for polymers whose modulus and hardness are measured, the values of l_R and m in Table 2 are respectively greater than those in Table 1. Especially, in Table 2 the l_R of PAI reaches about 500 nm and that of LDPE can even reach near 90000 nm. The m value of LDPE in Table 2 can even reach 2.9 which significantly deviates from the theoretical range of m.

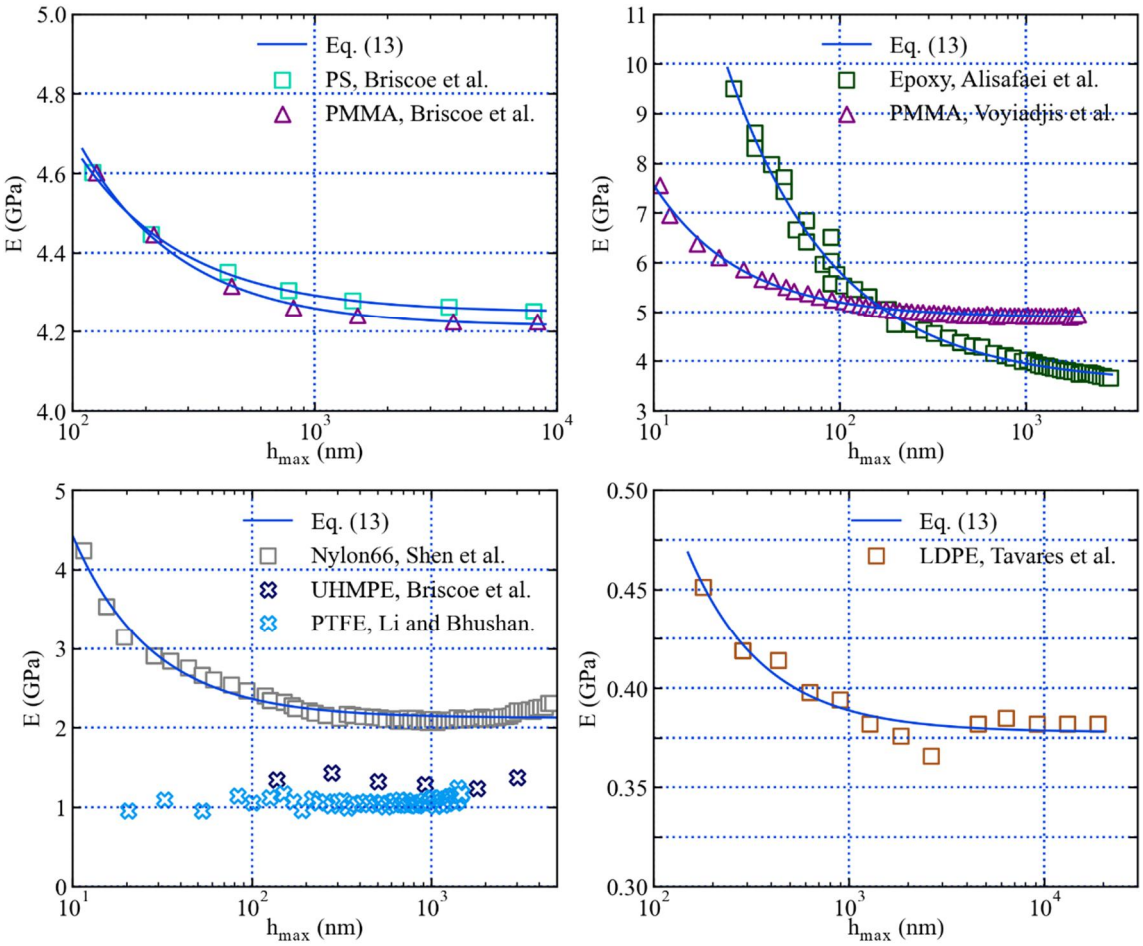

Fig. 4. The scattering points are experimentally obtained indentation moduli of PS (Briscoe et al. [3]), PMMA (Briscoe et al. [3]; Voyiadjis et al. [10]), Epoxy (Alisafaei et al. [8]), Nylon66 (Shen et al. [6]), UHMWPE (Briscoe et al. [3]), PTFE (Li and Bhushan [24]) and LDPE (Tavares et al. [5]); The solid lines are fitting results of Eq. (13) to the experimental data with size effects.

Table 1

Values of E_0, l_R and m obtained by fitting Eq. (13) to the size-dependent experimental data in Fig. 4.

Experimental data	E_0 (GPa)	l_R (nm)	m	Experimental data	E_0 (GPa)	l_R (nm)	m
PS (Briscoe et al.)	4.25	28.6	1.49	PMMA (Voyiadjis et al.)	4.87	13.7	1.44
PMMA (Briscoe et al.)	4.21	41.6	1.53	Nylon66 (Shen et al.)	2.06	22.2	1.48
Epoxy (Alisafaei et al.)	3.55	49.3	1.25	LDPE (Tavares et al.)	0.38	177.5	1.59

Table 2

Values of H_0, l_R and m obtained by fitting Eq. (15) to the size-dependent experimental data in Fig. 5.

Polymers	H_0 (GPa)	l_R (nm)	m	Polymers	H_0 (GPa)	l_R (nm)	m
PS (Briscoe et al.)	0.26	58.27	1.63	PMMA (Voyiadjis et al.)	0.29	20.42	1.54
PMMA (Briscoe et al.)	0.25	93.70	1.71	Nylon66 (Shen et al.)	0.09	42.33	1.55
Epoxy (Alisafaei et al.)	0.2	181	1.66	LDPE (Tavares et al.)	0.025	87841	2.90
Epoxy (Chong and Lam)	0.25	7.53	1.15	PC (Chong and Lam)	0.15	6.27	1.06
PAI (Tatiraju et al.)	0.13	511	1.41	PC (Samadi-Dooki et al.)	0.21	14.55	1.25

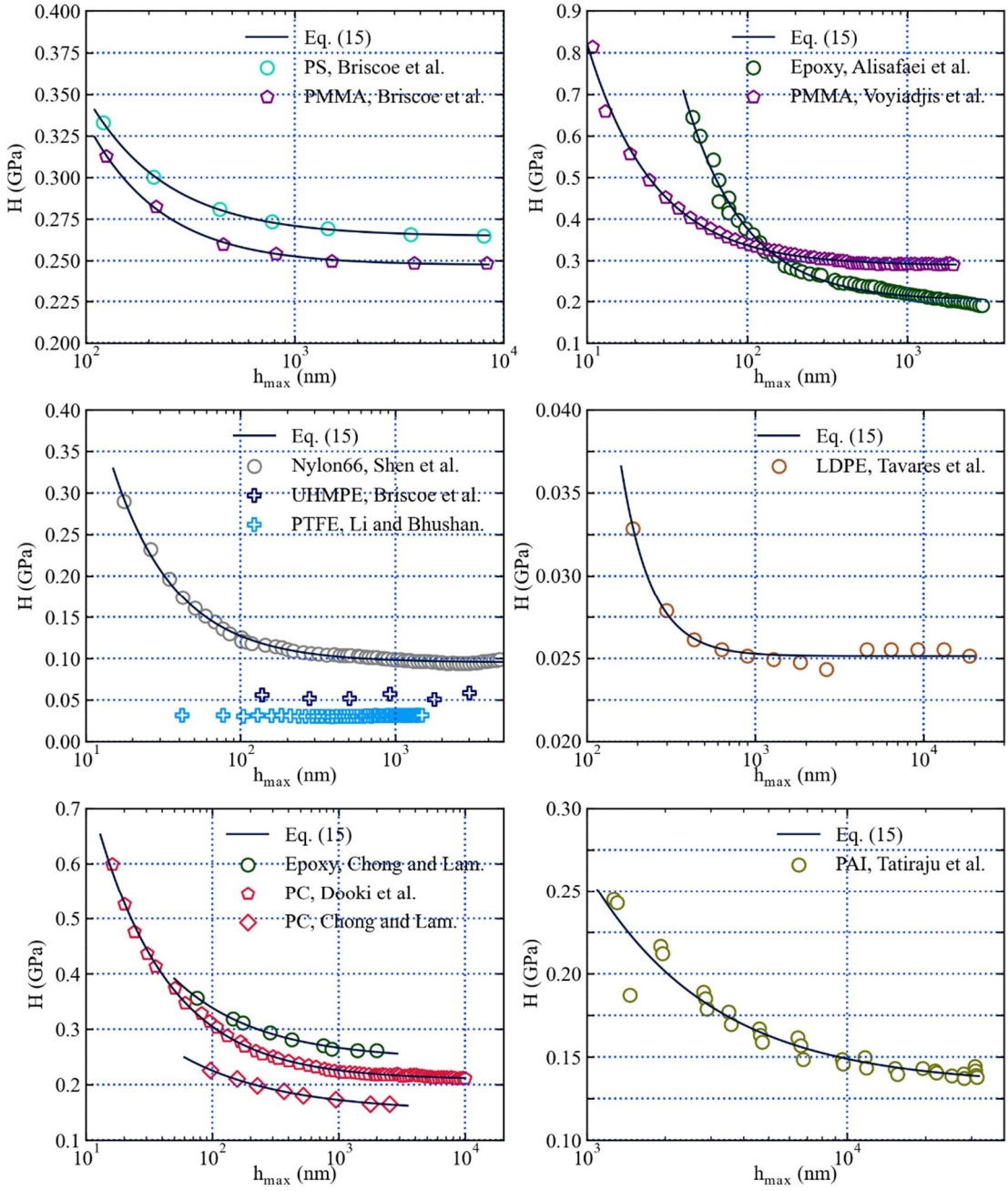

Fig. 5. The scattering points are experimentally obtained indentation hardness of PS (Briscoe et al. [3]), PMMA (Briscoe et al. [3]; Voyiadjis et al. [10]), Epoxy (Alisafaei et al. [8]; Chong and Lam [4]), Nylon66 (Shen et al. [6]), UHMWPE (Briscoe et al. [3]), PTFE (Li and Bhushan [24]), LDPE (Tavares et al. [5]), PC (Samadi-Dooki et al. [9]; Chong and Lam [4]) and PAI (Tatiraju et al. [7]); The solid lines are fitting results of Eq. (15) to the experimental data with size effects.

2.3 Discussion

Before proceeding to the discussion of results in Table 1 and Table 2, let us discuss the influences of characteristic length l and elastoplastic properties of polymers on l_R and m, because these features of different polymers are significantly discrepant. Regarding to the characteristic length l of polymers, Nikolov et al. [25] and Han [26] have studied its physical mechanisms and related it to the bending stiffness of polymeric chains. The phenomenological rotation gradient energy in couple stress elasticity is related by Nikolov et al. [25] to the Frank elasticity energy, which is always present as long as the chains possess finite bending stiffness and neighboring interactions. They worked out a relation: $K = 3\mu l^2$ linking the phenomenological characteristic length l to the effective Frank

elasticity constant K. Han [26] subsequently illustrated in detail the dependence of characteristic length l on the molecular bending stiffness, although the exact l value of each polymer is not estimated. They found that polymers containing complex molecular structures in chains always have larger characteristic length l than those having flexible chains. For example, PAI, Epoxy, PC and PS have the longest l due to the stiffening of aromatic rings in the backbone or side group; PMMA and Nylon66 have shorter l, since PMMA has complex side groups and the Nylon66 has stiff areas of chains due to the presence of the O and N atoms [12], although they both lack aromatic rings; UHMWPE and PTFE have shortest l which can even be close to 0 nm due to their highly flexible and linear chains. LDPE was not considered in the work of Han [26]. The l of LDPE is presently considered to be longer than those of UHMWPE and PTFE due to its easily branched chains, but shorter than those of other polymers due to the flexibility of chains.

The elastoplastic properties of polymers mainly influence the parameter η_e which denotes the fraction of elastic recovery in total elastoplastic deformation depth. In general, polymers with higher cross-link/entanglement density can provide higher elastic resistance than those containing flexible chains, because the flexible chains can easily adjust themselves to plastically dissipate the indentation work [26]. This kind of dependence is approximately consistent with the dependence of characteristic length l on the molecular bending stiffness. As can be seen in Fig. 3, the fraction of elastic work of PAI is larger than those of other polymers, and the corresponding fraction of UHMWPE is the lowest. According to the definition of η_e in Section 2.1, it can be postulated that the parameter η_e also approximately conforms the size sequence of molecular stiffness. Additionally, the results of finite element simulations for a variety of elastic to plastic materials [21] show that the exponent m obviously increases with decreasing η_e. Furthermore, according to the analytical solutions of Sneddon [20], the increasing m implies that the effective shape of indenter is close to a cone, resulting in a smaller effective curvature radius R.

The l_R and m values in Table 1 are consistent with the above considerations. According to the mathematic form of Eq. (14), the l_R increases with increasing l, however decreases with increasing η_e. This is the reason why the l_R values in Table 1 do not strictly conform the size sequence of l. For example, the PS and Epoxy containing rigid aromatic rings in chains should theoretically have the largest l_R than other polymers, but their η_e value may also be the largest, thus the resulted l_R value is not the largest one. For LDPE, if its η_e value is considered to be close to that of UHMWPE, it also has the lowest η_e value. According to the finite element simulations of Pharr and Bolshakov [21] mentioned above, its lowest η_e causes the largest m value among these polymers. More importantly, the lowest η_e and the largest m of LDPE, along with the correspondingly smaller effective curvature radius R, make the resulted l_R value the largest among these polymers, although the LDPE has a shorter l than them. Conclusively, with these considerations, the results shown in Fig. 4 and Table 1 demonstrate that the modulus model Eq. (13) can be successfully applied to characterize the modulus ISEs of polymers.

The corresponding deviations between the values of l_R and m in Table 2 and those in Table 1 can be attributed to the discrepancy that the experimentally obtained hardness ISEs contain both elastic part and plastic part, while Eq. (15) considers only the elastic part. As discussed above, the plastic dissipation of LDPE in indentation is significant due to its relatively flexible chains, thus the plastic hardness ISEs of LDPE may even be dominant. This is exactly the reason why the values of l_R and m of LDPE significantly deviate from those predicted by Eq. (13), and from the theoretical range. For other polymers in Table 1, the fraction of plastic deformation is smaller than that of LDPE, thus the plastic hardness ISEs are slighter than those of LDPE. Therefore, the corresponding deviations are not as significant as that of LDPE. It can even be postulated that for all polymers shown in Fig. 5, if the elastic hardness ISEs can be separated from the experimental data and fitted by Eq. (15), the same values of l_R and m as those predicted by Eq. (13) will be obtained. That is to say, despite these deviations, the hardness model Eq. (15) can still be applied to characterize the elastic hardness ISEs. In particular, the PAI has the lowest fraction of plastic deformation among all polymers. Therefore, the plastic hardness ISEs of PAI may be trivial. If its modulus data are

obtained by experiment and fitted by Eq. (13), the same values of l_R and m as their counterparts (estimated by Eq. (15)) in Table 2 will be obtained.

The influences of the plastic hardness ISEs can also be explicitly reflected by relation Eq. (16). For each polymer depicted in Fig. 4, the $(E-E_0)/E_0$ values where E_0 comes from Table 1 are plotted versus $1/h_{max}$ in Fig. 6. The corresponding $(H-H_0)/H_0$ values where H_0 comes from Table 2 are also plotted. According to the discussion of Eq. (16) in Section 2.1, for each polymer whose m values in both Table 1 and Table 2 are uniformly close to 1.5, the data points of either $(H-H_0)/H_0$ or $(E-E_0)/E_0$ will line up more straightly. Additionally, a triple relation will exist between the slopes of the two linear trends. For a more explicit comparison, a straight line passing through the point (0, 0) is respectively fitted to these data points. As can be seen in Fig. 6, this kind of tendency is approximately reflected by the data points of PS, PMMA, and Nylon66. As deviant E_0 and H_0 values are predicted for Epoxy (Alisafaei et al. [8]) in Fig. 4 and Fig. 5, its data points in Fig. 6 slightly deviate from the liear tendency. However, it can be found that the data points of LDPE significantly deviate the linear trend. The corresponding slopes of these linearly fitting are shown in Table 3. As can be seen therein, for PS, PMMA and Nylon66, the triple relation is obvious. However, for LDPE the relation in slopes significantly deviates from the triple relation, which can be exactly attributed to the significant fraction of plastic hardness ISEs. Finally, it is noted that the linear fits in Fig. 6 are adopted to illustrate not the validities of Eq. (13) and Eq. (15) (both for choice m = 1.5), but the influence of plastic hardness ISEs on the validities of the two models.

All results present above indicate that for polymers shown in Fig. 5 other than LDPE, the hardness ISEs are significantly elastic, while the hardness ISEs of LDPE are significantly plastic. Additionally, these results yield the presentiment that if the plastic hardness ISEs are to be characterized by a model, this model may be in a similar mathematical form to Eq. (15), but with an exponent larger than $m-0.5$. Firstly, as can be seen in Fig. 5, although the experimentally obtained hardness of all polymers have already contained plastic ISEs, the mathematical form of Eq. (15) can still give an exact graphical description of the whole hardness ISEs. This implies the plastic hardness ISEs can also be described by a formula in the similar form to Eq. (15), i.e., the augmenting effect term is proportional to the power of $1/h_{max}$. Secondly, for polymers whose moduli are also measured, the m value estimated by the Eq. (15) is respectively larger than those estimated by the modulus model Eq. (13). This implies that the corresponding exponent in plastic hardness ISEs will be larger than $m-0.5$. According to the fitted results of LDPE, this exponent may be larger than 2.4. Thirdly, this inference is compatible with a categorization of the hardness ISEs suggested by Han (2010), which says that for a polymer the depth range presenting elastic hardness ISEs is always larger than that presenting the ISEs mediated by other factors. It can be easily seen from Eq. (15) that as the exponent $m-0.5$ becomes larger, the augmenting term will become smaller at the depths beyond $\sqrt[m-0.5]{l_R}$, and larger at the depths within $\sqrt[m-0.5]{l_R}$. That is to say, at the depths beyond $\sqrt[m-0.5]{l_R}$ the elastic hardness ISEs will be more obvious than the plastic hardness ISEs, and consequently more easily observed by experiments.

Finally, the non-existence of hardness ISEs of UHMWPE and PTFE yields the presentiment that the plastic hardness ISEs of semi-crystalline polymers may be derived from only their glassy components, but not their crystal components. In indentation, the plastic deformation zone is only the region beneath the indenter. In semi-crystalline polymers, the deformations begin with the elastic and subsequently plastic deformations of glassy components [27]. In a local region, after glassy components are exhausted, the deformations are transferred to the crystal components by various crystallographic processes up to large plastic strains. UHMWPE and PTFE have the highest degree of crystallinity due to their highly linear chains, thus their plastic deformations beneath the indenter are mainly derived

from crystal components. However, as can be seen from Fig. 5, both UHMWPE and PTFE exhibit no hardness ISEs. This indicates that the plastic deformation of their crystal components mediates no size effect. It can be postulated that for semi-crystalline Nylon66 and LDPE, the plastic deformation of crystal components may also mediate no size effect, and thus their plastic hardness ISEs are only related to glassy components.

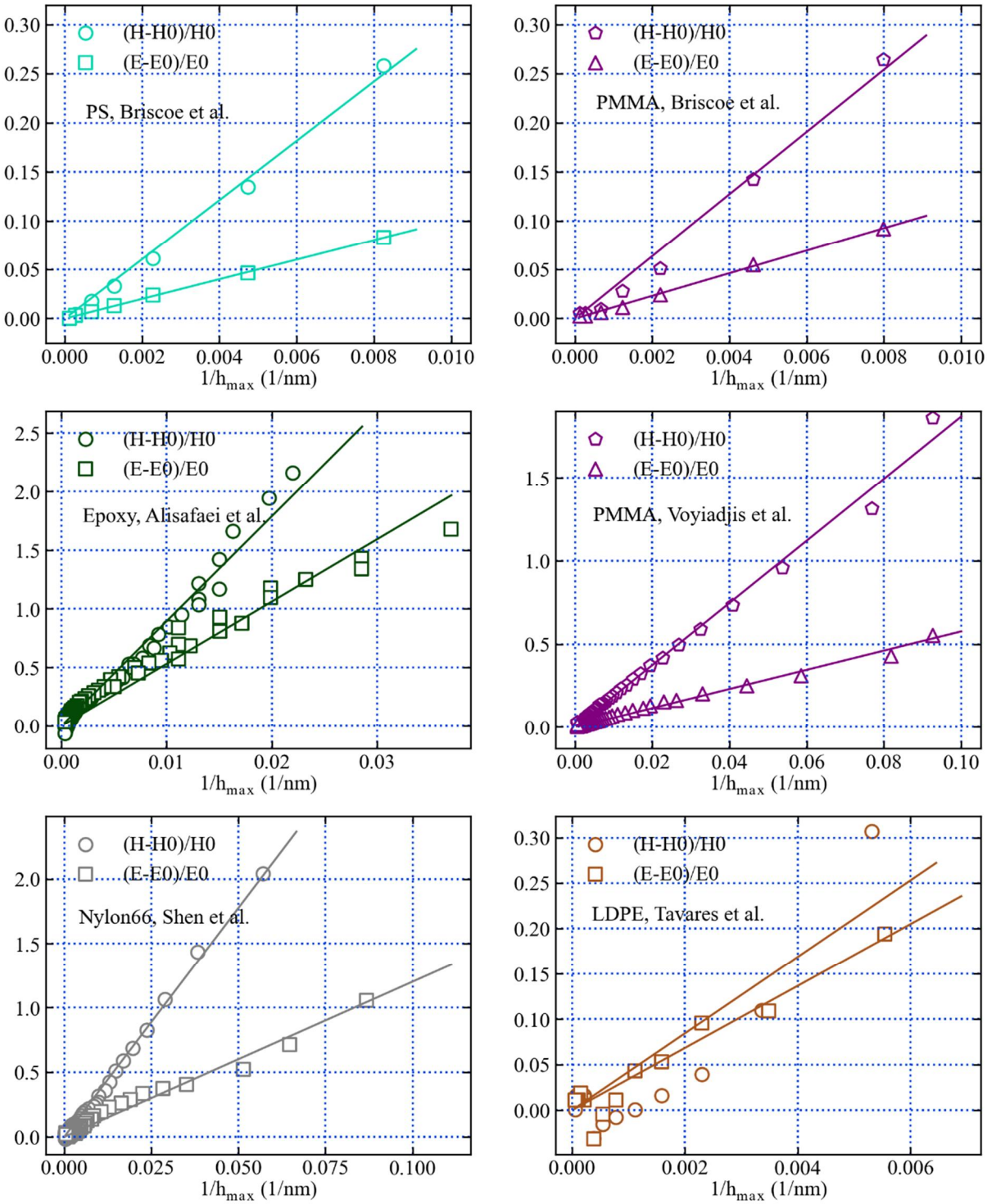

Fig. 6. Values of $(E-E_0)/E_0$ and $(H-H_0)/H_0$ of the polymers depicted in Fig. 4, respectively plotted with respect to $1/h_{\max}$. The E_0 value and H_0 value of each polymer respectively come from Table 1 and Table 2. A straight line passing through (0, 0) is respectively fitted to these data points.

Table 3

Slopes obtained by linearly fitting the data points in Fig. 6.

Linearly fitted slopes	PS	PMMA	Epoxy (Alisafaei et al., 2014)	PMMA (Voyiadjis et al., 2018)	Nylon66	LDPE
$(H-H_0)/H_0$	30.26	31.79	89.47	18.68	35.51	42.21
$(E-E_0)/E_0$	10.02	11.56	53.11	5.77	12.02	36.52

3. Models for the plastic indentation size effects of polymers

This section attempts to model the plastic hardness ISEs of polymers. Studies in this respect mainly involve incorporating size characteristic into the formula of plastic deformation. Lam and Chong [11] developed a strain gradient plasticity theory and a corresponding hardness model, based on the molecular kink pair theory of Argon [28] in which the carrier of plasticity is the formation of kink pairs. Their hardness model, similar to that of Nix and Gao [2] for crystals, employs the notion of statistically random kinks and geometrically necessary kinks of chains. However, in Argon's plasticity theory for glassy polymers, the carrier of plasticity has been replaced by the nucleation of shear transformations (STs) [29, 14, 10] which was originally proposed by Argon for glassy metals[30, 31]. The STs represent the cooperative rearrangements of atoms inside some free volume sites under the enforcing of shear stress, including gliding, slipping, or shear rotation of the chains. The massive nucleation of shear transformation events results in the stable plastic flow of glassy metals. Based on the notion of STs, a plastic constitutive formula was developed by Voyiadjis and Samadi-Dooki [14] for PMMA. Their constitutive formula shows its success in not only capturing the primary softening behavior, but also justifying the secondary hardening observed in compressive experiments of PMMA. Voyiadjis et al. [10] subsequently interpreted the ISEs of glassy polymers as that the probability of nucleating STs with average size, at the very small indentation depths, is lower than that at deep indentation depths, and consequently, higher shear stresses are caused. This probabilistic interpretation of ISEs provides a novel insight to understand the plastic ISEs of polymers.

3.1. Model development

The constitutive formula of Voyiadjis and Samadi-Dooki [14] is briefly recalled here. In unstressed state, a large amount of free volume sites with different sizes are distributed in the microstructure due to the amorphous nature of glassy polymers. Among these free volume sites, those with excessive free volume are more likely to foster atomic STs under enforcing of shear stress, as shown in Fig. 7. These sites with excessive free volume are also called potential transformation sites, which are only a fraction of all free volume sites. It is noted that the STs are not any existing defects but dynamic events only instantaneously nucleating under enforcing of shear stress. Those potential transformation sites where the ST events are occurring are called shear transformation zones (STZs) (see Fig. 7). The STZs have a characteristic average volume Ω and a characteristic shear strain γ^{T}.

The constitutive relation between the global shear strain rate $\dot{\gamma}^{P}$ and global shear yield stress τ is expressed as

$$\dot{\gamma}^{P}=\dot{\gamma}_0^{P} c_{\mathrm{f}} \exp\left(\frac{-\Delta F}{k_{\mathrm{B}}T}\right)\sinh\left(\frac{\gamma^{\mathrm{T}}\Omega\tau}{2k_{\mathrm{B}}T}\right), \tag{17}$$

where k_{B} is Boltzmann constant, T is absolute temperature, the pre-exponential $\dot{\gamma}_0^{P}$ can be calculated by $\gamma^{\mathrm{T}}\nu_{\mathrm{G}}$ with ν_{G} being the frequency of atomic vibration (~ Debye frequency) in the range of $10^{10}\,\mathrm{s}^{-1}$, ΔF is the average nucleating energy of STs, and c_{f} is a factor depending on the volume fraction of potential transformation sites. The average nucleating energy of STs with shear strain of γ^{T} and average volume of Ω, is considered equal to the deformation energy in the inclusion model of Eshelby [32] and expressed as

$$\Delta F = f(\nu,\beta)\mu(\gamma^{\mathrm{T}})^2\Omega, \tag{18}$$

where μ is the shear modulus, and $f(\nu,\beta)$ accounts for shear and dilatational components of the transformation

strain tensor. For polymers with the Poisson's ratio of 0.35-0.4, $f(\nu,\beta)$ has a value close to 0.5 [14, 10].

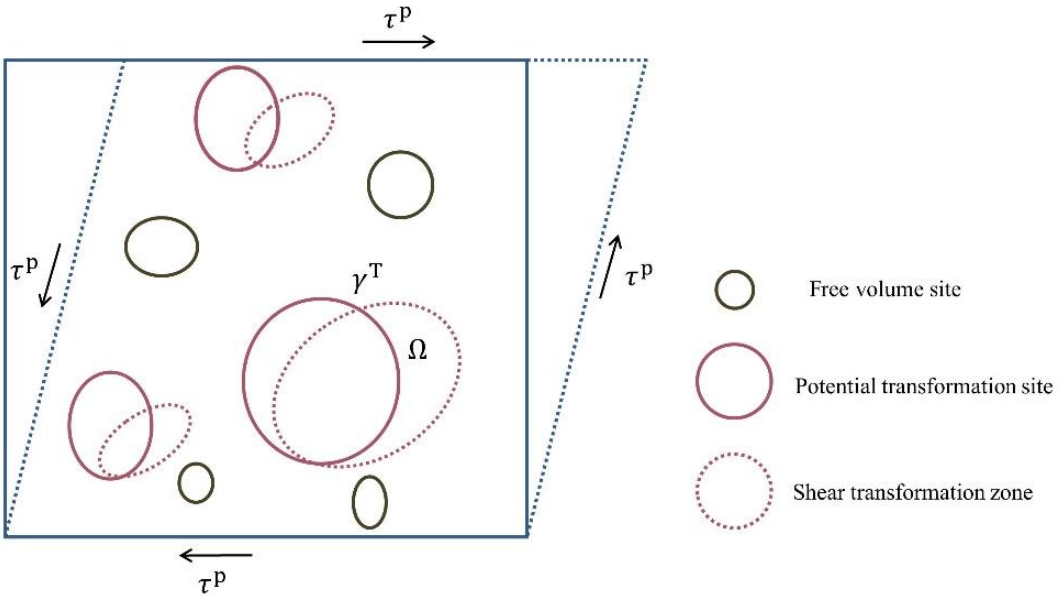

Fig. 7. The representative free volume sites in glassy polymers and the corresponding shear transformation events nucleated inside some sites.

Voyiadjis et al. [10] subsequently interpreted the indentation size effects of glassy polymers based on the above constitutive formula. They suggested that the nucleation of STs in the deformation zone beneath the indenter is a probabilistic phenomenon. On one hand, the size of a unit potential transformation site could be manifested as a spherical region with a diameter of about 10 nm, on the other hand, the potential transformation sites are only a fraction of all free volume sites and discretely distributed in the material. Therefore, at very small indentation depths, the deformation zone is not big enough to "see" a potential transformation site, and thus atoms in this zone can hardly rearrange themselves (shear transformation) to dissipate the indentation work, as schematically in Fig. 8(a), consequently the corresponding deformation zone is highly stressed. As the indenter continues to move down, the region around the highly stressed zone starts to "see" potential transformation sites and form ST events (Fig. 8(b)). At very deep indentation depths, the ST events could massively nucleate and control the kinetics of deformation (Fig. 8(c)).

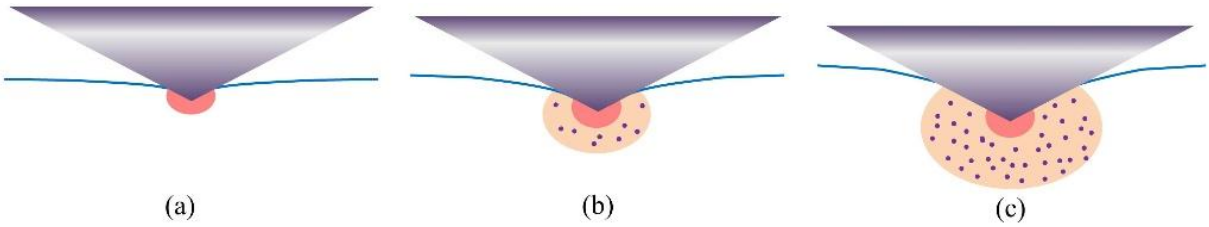

Fig. 8. The diagram for the distribution of shear transformation zones along the indentation depth.

They suggested that the total shear stress in the whole deformation zone can be decomposed into two parts. One is the shear stress associated with nucleation of a single ST, the other is the shear stress associated with the plastic deformation of the highly stressed region, respectively denoted as τ_{ST} and τ_{local}. The τ_{ST} is derived from Eq. (17) where the parameter $\gamma^{\mathrm{T}}\Omega\tau$ is considered to be far larger than the unit thermal activation energy $k_{\mathrm{B}}T$ for polymers at temperatures below their glass transition, and the fraction parameter c_{f} is set to 0.5. Then the τ_{ST} is expressed as

$$\tau_{\mathrm{ST}}=\frac{2k_{\mathrm{B}}T}{\gamma^{\mathrm{T}}\Omega}\left[\ln\left(\frac{4\dot{\gamma}^{P}}{\dot{\gamma}_{0}^{P}}\right)+\frac{\mu(\gamma^{\mathrm{T}})^{2}\Omega f(\nu,\beta)}{k_{\mathrm{B}}T}\right]. \tag{19}$$

The τ_{local} is obtained by directly setting Ω in Eq. (19) to the size of the plastic deformation zone. The plastic deformation zone is assumed to be the hemisphere under the indenter with subtracting the volume of the pyramidal indenter itself. Its size is identified to be $164h_{\max}^3$.

The total shear stress is expressed in a statistical form of the above stress components. To this end, they extended the fraction parameter c_{f} to the probability of the nucleation of STs and also the probability of τ_{ST} in the statistical form. This probability is specifically expressed as

$$c_{\text{f}} = \exp(\frac{-k\Omega}{h_{\max}^3}), \tag{20}$$

where k is a dimensionless fitting parameter, accounting for indenter geometry, proportionality and free volume fraction. As can be seen in Eq. (20), the probability quantitatively decreases with the decreasing indentation depths. As the indentation is implemented at deeper depths, the probability increases and has an upper limit of 1, representing the massive nucleation of STs. With this probability, they expressed the total shear stress as

$$\tau_{\text{total}} = c_{\text{f}}\tau_{\text{ST}} + (1-c_{\text{f}})\tau_{\text{local}}. \tag{21}$$

Then the hardness model is expressed by Voyiadjis et al. [10] as

$$H = \frac{13.2k_{\text{B}}T}{\gamma^{\text{T}}}\left[\frac{c_{\text{f}}}{\Omega}\left(\ln\left(\frac{4\dot{\gamma}^{P}}{\dot{\gamma}_0^{P}}\right)+\frac{\mu(\gamma^{\text{T}})^2\Omega f(\nu,\beta)}{k_{\text{B}}T}\right)+\frac{1-c_{\text{f}}}{164h_{\max}^3}\left(\ln\left(\frac{4\dot{\gamma}^{P}}{\dot{\gamma}_0^{P}}\right)+\frac{164h_{\max}^3\mu(\gamma^{\text{T}})^2 f(\nu,\beta)}{k_{\text{B}}T}\right)\right], \tag{22}$$

where the relation $H = 6.6\tau_{\text{total}}$ [33] for polymers is considered, similar to Tabor's relation [34] for metals.

However, the hardness model Eq. (22) is too complex for application. Additionally, the estimation of τ_{local} (the non-ST mediated stress), i.e., directly substituting the size of a STZ in τ_{ST} for the size of the whole deformation zone, needs more rationalities. A size effect model can be directly derived from the constitutive formula Eq. (17), because Eq. (17) itself has already contained the probability parameter, or presently called size effect factor c_{f}. Similarly, considering that the parameter $\gamma^{\text{T}}\Omega\tau$ is far larger than $k_{\text{B}}T$, Eq. (17) can be converted to

$$\tau = \frac{2k_{\text{B}}T}{\gamma^{\text{T}}\Omega}\left[\ln\left(\frac{2\dot{\gamma}^{P}}{\dot{\gamma}_0^{P}}\right)+\frac{\mu(\gamma^{\text{T}})^2\Omega f(\nu,\beta)}{k_{\text{B}}T}+\frac{k\Omega}{h_{\max}^3}\right]. \tag{23}$$

It can be seen that the indentation size has been successfully introduced into the constitutive formula. With the relation $H = 6.6\tau$ [33] a hardness model can be expressed as

$$H = \frac{13.2k_{\text{B}}T}{\gamma^{\text{T}}\Omega}\left[\ln\left(\frac{2\dot{\gamma}^{P}}{\dot{\gamma}_0^{P}}\right)+\frac{\mu(\gamma^{\text{T}})^2\Omega f(\nu,\beta)}{k_{\text{B}}T}\right]+\frac{13.2k_{\text{B}}kT}{\gamma^{\text{T}}h_{\max}^3}, \tag{24}$$

where the last term denotes the STs plasticity mediated hardness ISEs. When the indentation is implemented at far deeper depths, the STs are massively nucleated and the hardness augment tends to be 0. It can be seen that Eq. (24) has a simpler form than Eq. (22), although with the same number of parameters as Eq. (22).

The hardness model Eq. (24) can be rewritten as

$$H = H_0\left[1+\frac{V_\Omega}{h_{\max}^3}\right] \tag{25}$$

where the parameter V_Ω is expressed as

$$V_\Omega = k\Omega/\left[\ln\left(\frac{2\dot{\gamma}^{P}}{\dot{\gamma}_0^{P}}\right)+\frac{\mu(\gamma^{\text{T}})^2\Omega f(\nu,\beta)}{k_{\text{B}}T}\right], \tag{26}$$

and the macro hardness H_0 is expressed as

$$H_0 = \frac{13.2 k_B T}{\gamma^T \Omega}\left[\ln\left(\frac{2\dot{\gamma}^P}{\dot{\gamma}_0^P}\right) + \frac{\mu(\gamma^T)^2 \Omega f(\nu,\beta)}{k_B T}\right]. \tag{27}$$

It can be found that Eq. (25) has a similar form to Eq. (15) which characterizes the elastic hardness ISEs. More importantly, the exponent of $1/h_{max}$ in Eq. (25) is 3, being larger than the exponent $m-0.5$ in Eq. (15). These two features are well consistent with the inference in the end of Section 2.3. As discussed therein, if the plastic hardness ISEs are to be characterized, the corresponding hardness model should have a similar form to Eq. (15), but with an exponent larger than $m-0.5$. Additionally, a dimensional analysis to Eq. (26) suggests that the parameter V_Ω has a dimension of volume. This parameter can be seen as a higher-order volume parameter similar to the higher-order length parameter l_R in Eq. (15).

3.2. Model verification and discussion

In principle, the validity of model Eq. (25) should be illustrated by hardness data containing only plastic ISEs. However, to separate the plastic ISEs from hardness data of polymers in Fig. 5 is impossible. A compromise is applying it to the hardness data of LDPE in which the plastic ISEs are dominant. As shown in Fig. 9(a), a good agreement between the model and the experimental data is found. The macro hardness H_0 and volume parameter V_Ω are respectively estimated to be about 0.025 GPa and 2×10^6 nm^3. Then the characteristic volume Ω of STZ is estimated to be about 2718 nm^3 (for choice $\gamma^T = 0.04$) and parameter k is estimated to be about 5×10^4, respectively from Eq. (27) and Eq. (26). Taking the obtained Ω and k into Eq. (20), the varying probability of nucleating STs with respect to h_{max} is depicted in Fig. 9(b). It can be seen that the probability curve is compatible with the hardness curve. When the indentation is implemented in small depths, the deformation zone is too small to foster a ST event. As the indenter continues to move down, the probability is close to 1 which implies the massive nucleation of STs, and thus the hardness value correspondingly tends to be stable.

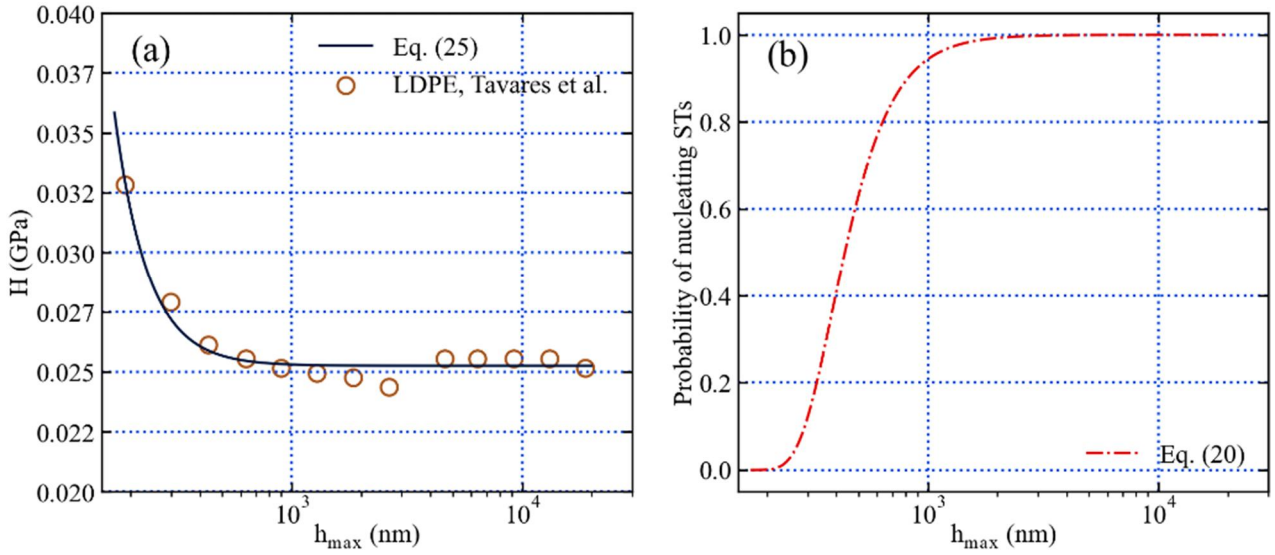

Fig. 9. (a) Fitting the hardness model Eq. (25) to the experimentally obtained hardness of LDPE (Tavares et al. [5]); (b) The probability of nucleating STs versus indentation depths obtained by substituting the fitted values of Ω and k into Eq. (20).

The presently obtained Ω of LDPE is close to the STZ volumes of several other polymers given by Mott et al.

[35] through molecular simulations, which range from hundreds to thousands of cubic nanometers. The presently obtained k also has the same order of magnitude as that of PMMA estimated by Voyiadjis et al.[10]. Note that the determination of Ω is significantly sensitive to the chosen value of γ^{T}, for example, the Ω will be 1183 nm^3 for choice $\gamma^{\mathrm{T}} = 0.05$. The γ^{T} of PMMA is believed to be in the range of 0.03 to 0.05 by the interpolation of experimental data (Malekmotiei et al. [36]; Voyiadjis et al.[10]), and thus the middle of this range is adopted in the present estimation. The temperature T is set at 295 K for room temperature experiments, as Tavares et al. [5] did not specify that the experiments were carried out under heating or cooling conditions.

The shear strain rate $\dot{\gamma}^{P}$ has been found to alter the macro hardness [10], as illustrated in Eq. (27). However, its contribution is not able to justify the observed indentation size effect in hardness[33], although it emerges into the higher-order volume parameter V_{Ω}. In above estimation of Ω, the value of $\dot{\gamma}^{P}$ is obtained from $\dot{\gamma}^{P} = \sqrt{3}C\dot{\varepsilon}_i$ where C is a constant value equal to 0.09 and $\dot{\varepsilon}_i$ the indentation strain rate [38, 36]. Tavares et al. [5] did not provide the indentation strain rate $\dot{\varepsilon}_i$, but stated that a high rate was adopted to minimize the influence of viscoelastic properties in the measurements. The above estimation assumes $\dot{\varepsilon}_i$ to be 1 s^{-1}. Additionally, the shear modulus μ is obtained from $2\mu = E/(1+\nu)$ where $\nu = 0.4$ [39] and E is the macro modulus in Table 1 as Eq. (27) denotes the macro hardness.

4. Conclusions

The size effects in indentation modulus (modulus ISEs) and indentation hardness (hardness ISEs) of polymers are theoretically modeled, on the basis of literatures which found that the modulus ISEs are elastic and the hardness ISEs can be divided into elastic part and plastic part in which the elastic part is likely to be dominant. The modulus ISEs and the elastic hardness ISEs are modeled, by introducing a couple stress elasticity-based unloading model proposed in our previous work into Oliver-Pharr indentation approach. The resultant modulus model and hardness model, along with the corresponding results of application to experimental data, show that these elastic size effects and their experimental showing are mainly determined by the molecular structures. Specifically, polymers with complex molecules would exhibit significant modulus ISEs. Besides, the hardness ISEs of this kind of polymers are significantly elastic.

The couple stress elasticity-based hardness model shows a shortage in characterizing the hardness ISEs of LDPE. We postulate that the hardness ISEs of LDPE are significantly plastic, due to its highly flexible molecular structures. As both the UHMWPE and PTFE with high crystallinity exhibit no indentation size effects, we postulate that the plastic hardness ISEs of polymers are only determined by their glassy components and may be described by a model in a similar form to that of the couple stress elasticity-based hardness model. Based on these considerations, the shear transformation plasticity theory proposed for amorphous solids is employed to characterize the plastic hardness ISEs of polymers. Accordingly, a hardness model is proposed and successfully applied to experimental data. Besides, the shear transformation plasticity-based hardness model is completely consistent with previous speculation.

Acknowledgements

The authors would like to thank the National Natural Science Foundation of China (51873051, 51790502) for the financial support of this research.

References

1. Oliver, W.C., Pharr, G.M.: An improved technique for determining hardness and elastic modulus using load and displacement sensing indentation experiments. J. Mater. Res. 7, 1564–1583 (1992). https://doi.org/10.1557/JMR.1992.1564
2. Nix, W.D., Gao, H.: Indentation size effects in crystalline materials: A law for strain gradient plasticity. J. Mech. Phys. Solids. 46, 411–425 (1998). https://doi.org/10.1016/S0022-5096(97)00086-0

3. Briscoe, B.J., Fiori, L., Pelillo, E.: Nano-indentation of polymeric surfaces. J. Phys. D Appl. Phys. 31, 2395–2405 (1998). https://doi.org/10.1088/0022-3727/31/19/006
4. Chong, A.C.M., Lam, D.C.C.: Strain gradient plasticity effect in indentation hardness of polymers. J. Mater. Res. 14, 4103–4110 (1999). https://doi.org/10.1557/JMR.1999.0554
5. Tavares, A.C., Gulmine, J. V, Lepienski, C.M., Akcelrud, L.: The effect of accelerated aging on the surface mechanical properties of polyethylene. Polym. Degrad. Stab. 81, 367–373 (2003). https://doi.org/10.1016/S0141-3910(03)00108-3
6. Shen, L., Liu, T., Lv, P.: Polishing effect on nanoindentation behavior of nylon 66 and its nanocomposites. Polym. Test. 24, 746–749 (2005). https://doi.org/10.1016/j.polymertesting.2005.04.004
7. Tatiraju, V.S., Han, C.-S., Nikolov, S.: Size dependent hardness of polyamide/Imide. Open Mech. J. 2, 89–92 (2008). https://doi.org/10.2174/1874158400802010089
8. Alisafaei, F., Han, C.-S., Lakhera, N.: Characterization of indentation size effects in epoxy. Polym. Test. 40, 70–78 (2014). https://doi.org/10.1016/j.polymertesting.2014.08.012
9. Samadi-Dooki, A., Malekmotiei, L., Voyiadjis, G.Z.: Characterizing shear transformation zones in polycarbonate using nanoindentation. Polymer (Guildf). 82, 238–245 (2016). https://doi.org/10.1016/j.polymer.2015.11.049
10. Voyiadjis, G.Z., Malekmotiei, L., Samadi-Dooki, A.: Indentation size effect in amorphous polymers based on shear transformation mediated plasticity. Polymer (Guildf). 137, 72–81 (2018). https://doi.org/10.1016/j.polymer.2018.01.006
11. Lam, D.C.C., Chong, A.C.M.: Indentation model and strain gradient plasticity law for glassy polymers. J. Mater. Res. 14, 3784–3788 (1999). https://doi.org/10.1557/JMR.1999.0512
12. Han, C.-S., Nikolov, S.: Indentation size effects in polymers and related rotation gradients. J. Mater. Res. 22, 1662–1672 (2007). https://doi.org/10.1557/JMR.2007.0197
13. Alisafaei, F., Han, C.S., Garg, N.: On couple-stress elasto-plastic constitutive frameworks for glassy polymers. Int. J. Plast. 77, 30–53 (2016). https://doi.org/10.1016/j.ijplas.2015.09.011
14. Voyiadjis, G.Z., Samadi-Dooki, A.: Constitutive modeling of large inelastic deformation of amorphous polymers: free volume and shear transformation zone dynamics. J. Appl. Phys. 119, 15 (2016). https://doi.org/10.1063/1.4953355
15. Gourgiotis P.A., Zisis Th., Giannakopoulos A.E.: Georgiadis H.G. The Hertz contact problem in couple-stress elasticity. Int. J. Solids. Struct. 2019, 168: 228-237
16. Zisis Th., Gourgiotis P.A., Baxevanakis K.P.: Georgiadis H.G. Some basic contact problems in couple stress elasticity. Int. J. Solids. Struct. 2014, 51:2084-2095
17. Wang Y.X., Zhang X., Shen H.M., Liu J., Zhang B.,Xu S.F.: Three-dimensional contact analysis with couple stress elasticity. Int. J. Mech. Sci., 2019, 153: 369-379
18. Gourgiotis P.A., Zisis Th.: Two-dimensional indentation of microstructured solids characterized by couple-stress elasticity. J. Strain Anal. Eng. 2016, 51(4): 318-331
19. Peng, C., Zeng, F.L., Yuan, B., Wang, Y.S.: An approximate model to describe the size effects of spherical contact tests, based on a modified couple stress elasticity. Acta Mech. 232, 4363–4377 (2021). https://doi.org/10.1007/s00707-021-03054-w
20. Sneddon, I.N.: The relation between load and penetration in the axisymmetric boussinesq problem for a punch of arbitrary profile. Int. J. Eng. Sci. 3, 47–57 (1965). https://doi.org/10.1016/0020-7225(65)90019-4
21. Pharr, G.M., Bolshakov, A.: Understanding nanoindentation unloading curves. J. Mater. Res. 17, 2660–2671 (2002). https://doi.org/10.1557/JMR.2002.0386
22. Hertz, H.: Ueber die Berührung fester elastischer Körper. J. für die reine und Angew. Math. 92, 156–171 (1882). https://doi.org/10.1515/crll.1882.92.156

23. Han, C.S., Sanei, S.H.R., Alisafaei, F.: On the origin of indentation size effects and depth dependent mechanical properties of elastic polymers. J. Polym. Eng. 36, 103–111 (2016). https://doi.org/10.1515/polyeng-2015-0030
24. Li, X., Bhushan, B.: Continuous stiffness measurement and creep behavior of composite magnetic tapes. Thin Solid Films. 377–378, 401–406 (2000). https://doi.org/10.1016/S0040-6090(00)01368-7
25. Nikolov, S., Han, C.-S., Raabe, D.: On the origin of size effects in small-strain elasticity of solid polymers. Int. J. Solids Struct. 44, 1582–1592 (2007). https://doi.org/10.1016/j.ijsolstr.2006.06.039
26. Han, C.-S.: Influence of the molecular structure on indentation size effect in polymers. Mater. Sci. Eng. A. 527, 619–624 (2010). https://doi.org/10.1016/j.msea.2009.08.033
27. Lin, L., Argon, A.S.: Structure and plastic deformation of polyethylene. J. Mater. Sci. 29, 294–323 (1994). https://doi.org/10.1007/BF01162485
28. Argon, A.S.: A theory for the low-temperature plastic deformation of glassy polymers. Philos. Mag. 28, 839–865 (1973). https://doi.org/10.1080/14786437308220987
29. Oleinik, E.F., Rudnev, S.N., Salamatina, O.B.: Evolution in concepts concerning the mechanism of plasticity in solid polymers after the 1950s. Polym. Sci. Ser. A. 49, 1302–1327 (2007). https://doi.org/10.1134/S0965545X07120073
30. Argon, A.S.: Plastic deformation in metallic glasses. Acta Met. 27, 47–58 (1979). https://doi.org/10.1016/0001-6160(79)90055-5
31. Argon, A.S., Shi, L.T.: Development of visco-plastic deformation in metallic glasses. Acta Metall. 31, 499–507 (1983). https://doi.org/10.1016/0001-6160(83)90038-X
32. Eshelby, J.D.: The determination of the elastic field of an ellipsoidal inclusion and related problems. Proc. R. Soc. Lond. A Math. Phys. Eng. Sci. 241, 376–396 (1957). https://doi.org/10.1098/rspa.1957.0133
33. Prasad, K.E., Keryvin, V., Ramamurty, U.: Pressure sensitive flow and constraint factor in amorphous materials below glass transition. J. Mater. Res. 24, 890–897 (2009). https://doi.org/10.1557/jmr.2009.0113
34. Tabor, D.: A simple theory of static and dynamic hardness. Proc. R. Soc. Lond. A Math. Phys. Sci. 192, 247–274 (1948). https://doi.org/10.1098/rspa.1948.0008
35. Mott, P.H., Argon, A.S., Suter, U.W.: Atomistic modelling of plastic deformation of glassy polymers. Philos. Mag. A. 67, 931–978 (1993). https://doi.org/10.1080/01418619308213969
36. Malekmotiei, L., Samadi-Dooki, A., Voyiadjis, G.Z.: Nanoindentation study of yielding and plasticity of poly (methyl methacrylate). Macromolecules. 48, 5348–5357 (2015). https://doi.org/10.1021/acs.macromol.5b01064
37. Voyiadjis, G.Z., Malekmotiei, L.: Variation of the strain rate during csm nanoindentation of glassy polymers and its implication on indentation size effect. J. Polym. Sci. Pt. B-Polym. Phys. 10, 2179–2187 (2016). https://doi.org/10.1002/polb.24127
38. Poisl, W.H., Oliver, W.C., Fabes, B.D.: The relationship between indentation and uniaxial creep in amorphous selenium. J. Mater. Res. 10, 2024–2032 (1995). https://doi.org/10.1557/JMR.1995.2024
39. Jee, A.-Y., Lee, M.: Comparative analysis on the nanoindentation of polymers using atomic force microscopy. Polym. Test. 29, 95–99 (2010). https://doi.org/10.1016/j.polymertesting.2009.09.009